

Determination of Venus' Interior Structure with EnVision

Pascal Rosenblatt, Caroline Dumoulin, Jean-Charles Marty, Antonio Genova

▶ **To cite this version:**

Pascal Rosenblatt, Caroline Dumoulin, Jean-Charles Marty, Antonio Genova. Determination of Venus' Interior Structure with EnVision. Remote Sensing, 2021, 13 (9), pp.1624. 10.3390/rs13091624 . hal-03429212

HAL Id: hal-03429212

https://nantes-universite.hal.science/hal-03429212

Submitted on 16 Nov 2021

HAL is a multi-disciplinary open access archive for the deposit and dissemination of scientific research documents, whether they are published or not. The documents may come from teaching and research institutions in France or abroad, or from public or private research centers.

L'archive ouverte pluridisciplinaire **HAL**, est destinée au dépôt et à la diffusion de documents scientifiques de niveau recherche, publiés ou non, émanant des établissements d'enseignement et de recherche français ou étrangers, des laboratoires publics ou privés.



Distributed under a Creative Commons Attribution 4.0 International License

remote sensing

MDPI

Technical Note

Determination of Venus' Interior Structure with EnVision

Pascal Rosenblatt [1,*], Caroline Dumoulin [1], Jean-Charles Marty [2] and Antonio Genova [3]

[1] Laboratoire de Planétologie et Géodynamique, UMR-CNRS6112, Université de Nantes, 44300 Nantes, France; caroline.dumoulin@univ-nantes.fr
[2] CNES, Space Geodesy Office, 31401 Toulouse, France; jean-charles.marty@cnes.fr
[3] Department of Mechanical and Aerospace Engineering, Sapienza University of Rome, 00184 Rome, Italy; antonio.genova@uniroma1.it
* Correspondence: pascal.rosenblatt@univ-nantes.fr

Abstract: The Venusian geological features are poorly gravity-resolved, and the state of the core is not well constrained, preventing an understanding of Venus' cooling history. The EnVision candidate mission to the ESA's Cosmic Vision Programme consists of a low-altitude orbiter to investigate geological and atmospheric processes. The gravity experiment aboard this mission aims to determine Venus' geophysical parameters to fully characterize its internal structure. By analyzing the radio-tracking data that will be acquired through daily operations over six Venusian days (four Earth's years), we will derive a highly accurate gravity field (spatial resolution better than ~170 km), allowing detection of lateral variations of the lithosphere and crust properties beneath most of the geological features. The expected 0.3% error on the Love number k_2, 0.1° error on the tidal phase lag and 1.4% error on the moment of inertia are fundamental to constrain the core size and state as well as the mantle viscosity.

Keywords: planetary interior structure; gravity field determination; deep space mission

check for updates

Citation: Rosenblatt, P.; Dumoulin, C.; Marty, J.-C.; Genova, A. Determination of Venus' Interior Structure with EnVision. *Remote Sens.* **2021**, *13*, 1624. https://doi.org/10.3390/rs13091624

Academic Editor: Giancarlo Bellucci

Received: 15 March 2021
Accepted: 19 April 2021
Published: 21 April 2021

Publisher's Note: MDPI stays neutral with regard to jurisdictional claims in published maps and institutional affiliations.

Copyright: © 2021 by the authors. Licensee MDPI, Basel, Switzerland. This article is an open access article distributed under the terms and conditions of the Creative Commons Attribution (CC BY) license (https://creativecommons.org/licenses/by/4.0/).

1. Introduction

Why Venus and Earth evolved so differently remains an open issue. The geological history of Venus is the most unknown among the terrestrial planets, preventing a full understanding of the processes that led to its current state. The primary objectives of the EnVision mission, candidate of the M5 call of the ESA's Cosmic Vision Programme, are to determine whether Venus is geologically active today and the possible atmospheric signature of this activity and its interior structure [1]. The knowledge of the planetary interior is needed to better constrain its cooling history [2–5] and its geological evolution. Since there is a lack of seismic data of moon(s) and of a global magnetic field, the unique way to constrain Venus' interior from core to crust is to determine an accurate and well-resolved gravity field and some dynamical information, such as the precession rate of its rotation axis.

The current solution of the Venus gravity field was determined from the radio tracking data of the NASA Magellan spacecraft [6,7] and additionally the Pioneer Venus Orbiter (PVO) [8,9] (the Venus Express spacecraft was almost not tracked during the lowest altitude part of its orbit, not allowing improvement of the resolution of the Magellan/PVO solution [10,11]). This recovered gravity field shows a non-uniform spatial resolution ranging from 540 to 170 km, preventing the full detection of the gravity signal induced by lithospheric loads, as well as crustal density and thickness variations. To improve the quality of Venus' gravity, it is fundamental to better understand the geological history of the planet [12]. In addition, our knowledge of the tidal component of the gravity field (i.e., the tidal Love number k_2) is limited by an uncertainty of 22% [13], which is not accurate enough to draw conclusions about Venus' deep interior structure, e.g., whether the core is solid (viscous) or liquid, what is its size and what is the viscosity of the mantle [14]. An

accurate estimation of these geophysical quantities would help to constrain the cooling history of the planet. Moreover, the gravity and the topography data can be used to estimate the crustal and elastic lithosphere thicknesses [12,15,16]. However, the spatial resolution of the gravity field solution from Magellan tracking data is below degree and order 70 (i.e., longer than 270 km) for almost half of the planet, yielding uncertainties in the crustal and lithosphere structure estimates [3]. The determination of the lithosphere thickness, especially of its elastic core, is important because it can be used to estimate the surface heat flux; this parameter is a key element in the thermal evolution of a planet [17,18].

Venus' surface exhibits several specific geological structures that are of interest to understand its past evolution; for instance, coronae, which are circular volcano-tectonic features commonly associated with plume-lithosphere interactions, that might be the location of subduction initiation [19]. Studying the evolution of these structures is then of deep interest to understand Venus' lithospheric rejuvenation. A recent geomorphological analysis has shown that several tens of coronae might be active today [20]. However, as pointed out by [21], only 25% of the coronae are gravity well-resolved. The average diameter of these features is about 210 km, and they are spread all over the globe [22], highlighting the importance of uniformizing the spatial resolution of the gravity field from Magellan to a value lower than 200 km.

The geophysical goals of the radio science experiment aboard EnVision are thus the determination of a uniform high-resolution gravity field to resolve anomalies associated with the geological features across the entire planet. Improved coverage of the planet will allow us to achieve an accuracy of the tidal Love number k_2 better than 3%, which is required to better constrain the Venus' mantle viscosity and composition (iron content) as well as the state of its core, by ruling out some combinations of these parameters in the current models of Venus interior [14]. The EnVision mission has two advantages with respect to the Magellan mission to meet these objectives: twice longer mission duration and twice better Doppler precision.

Here, we present numerical simulations of the EnVision gravity experiment to assess the quality of the Venus gravity solution that can be reached. Section 2 of this paper presents this experiment as currently designed; Section 3 displays the methodology to simulate this experiment; Section 4 shows the expected improvement of the Venusian gravity field and of the knowledge of the interior structure of the planet. Section 5 summarizes the main results.

2. Materials and Methods

2.1. The EnVision Gravity Experiment

The main technique to determine the gravity field of planets is based on the precise reconstruction of the motion of one or several orbiting spacecraft [8,23,24]. The Precise Orbit Determination (POD) process consists of fitting the dynamical model of the spacecraft motion to the radio-tracking data. The radiometric data are collected by Earth-based deep space stations [25] that enable the telecommunications to measure the Doppler shift of the radio-link carrier frequency. The spatial resolution and accuracy of the gravity field solution depend on the precision and coverage of the tracking measurements, as well as on the accuracy of the dynamical model and the spacecraft's orbital altitude.

The EnVision spacecraft orbit is an elliptical orbit with an altitude range between 220 km and 515 km and an inclination of 88 degrees allowing for high-resolution mapping of the Venus gravity field. The EnVision gravity experiment relies on the two-way radio link established on daily passages of at least 3.5 h long to guarantee the data download required by the EnVision payload. A very stable reference X-band frequency (at 7.1 GHz) is generated at the ground station and sent to the spacecraft, which then sends back to the station a coherent downlink frequency (X-band at 8.4 GHz) thanks to the radio-transponder of the spacecraft telecommunication system. An additional Ka-band downlink coherent frequency (32 GHz) is also sent back to Earth to support the telemetry volume

requirements. This two-way X/X-Ka radio link provides a precise Doppler tracking of the EnVision spacecraft over the six Venusian days of the mission science phase.

2.2. Methodology of Simulations

2.2.1. EnVision Doppler Noise Budget

The main source of noise in the X-band Doppler measurements between a Venusian spacecraft and the Earth is the electron content fluctuations of the interplanetary plasma along the propagation path of the radio wave (i.e., phase scintillation [26]). The noise amplitude depends on the Sun-Probe-Earth (SPE) angle: the smaller this angle is, the closer the radio-path to the solar corona is and the larger the noise is. Models enable the characterization of this noise [27], but only a multi-frequency link would enable a full calibration [28]. The EnVision tracking system provides a dual-frequency on the downlink only; thus, the plasma noise on the uplink remains. A floor value of 0.027 mm/s at 10 s Doppler count time is reached around inferior conjunctions (i.e., Venus is between the Sun and the Earth, Table A1), then increases toward superior conjunctions (i.e., the Sun is between the Earth and Venus), as a dominant source in the Doppler noise budget at SPE angles lower than 20 degrees (i.e., >0.1 mm/s, see Table A1). Solar conjunctions occur with a synodic period of 584 Earth days; therefore, two or three periods during the mission timespan (i.e., 1458 Earth days) will be characterized by high radio tracking noise, depending on the mission starting date with respect to the first superior conjunction (Figure A1).

In addition to the interplanetary plasma, other sources of propagation noise have to be taken into account due to the charged particles of the Earth's ionosphere and the propagation delay in the neutral atmosphere (troposphere). A calibration system using GNSS technics at the ESTRACK ground stations corrects the tropospheric effect with a residual error of 0.022 mm/s (see Table A1 and [29]). The same technics can also remove the ionosphere effect almost entirely. An additional source of noise is due to the frequency stability of the spacecraft radio-transponder. The current EnVision spacecraft design foresees a stability of 0.024 mm/s (Table A1), which is to be considered as a worse case compared to the Rosetta and Cassini transponders (1.7 and 4.3 times better, respectively [28]). However, it does not dominate the Doppler noise budget even at inferior conjunction periods (Table A1). Lower-level residual noise is due to the ground station Frequency and Time System [30] and its mechanical stability (Table A1 and [31]). The end-to-end Doppler noise budget, based on Table A1, is displayed in Figure A1 for the current design of the nominal science phase of the EnVision mission starting on 15 June 2035. It shows a total floor noise of 0.043 mm/s around the inferior conjunction periods and increases up to about 2.2 mm/s at the superior conjunction periods (Figure A1). The highest noise level is due to the interplanetary plasma effect, which largely dominates the other sources of noise around the superior solar conjunction in X-band and can reach a couple of mm/s due to the largest electron density fluctuations in the solar corona (see Figure 1 in [28]). For comparison, the X/X Doppler tracking data of Magellan had an average noise of around 0.1 mm/s at 10 s count time outside the superior conjunction period (see Figure 1 in [9]).

2.2.2. The EnVision Orbital Motion

An accurate dynamical model of the spacecraft orbital motion is also important to determine the gravity field of the planet [9,11,32–35]. Thorough modeling of all the forces driving the orbital motion of the EnVision spacecraft is taken into account. The primary effect is induced by Venus' gravitational force, including the tides exerted by the Sun on the planet (i.e., potential Love number k_2). The Love number k_2 has a real part and an imaginary part to take into account the tidal amplitude and the effect of the tidal phase lag, respectively (e.g., IERS conventions [36]). The Magellan/PVO gravity solution, expanded up to degree and order 180, and its associated Love number k_2 are assumed as initial knowledge in our simulations. We assumed a value of 0.295 for the real part and of 0.0059 for the imaginary part (i.e., tidal phase lag angle of 0.58°, corresponding to the median

value of the tidal dissipation factor Q values, expected from recent Venus interior structure models that assume various mantle composition, temperature and viscosity, as presented in [14]: see Figure 4 for this reference and Table A2). The gravitational perturbations induced on the spacecraft motion by the other planets of the solar system are also taken into account using a point-mass representation and planetary ephemerides [37].

The non-gravitational forces acting on the faces of the spacecraft include the atmospheric drag and the radiation pressure from the Sun and the planetary albedo and infra-red emission. A single value of the albedo and of the infra-red emission are here considered. We used the VTS3 model [38] for the density of the Venusian atmosphere at the altitudes of the EnVision spacecraft. To compute these non-gravitational forces, we used a cannonball shape model with a surface-to-mass ratio of 0.007 m^2/kg, which is representative of modern spacecraft design.

The numerical integration is performed by using these force models (hereafter *initial* model) over 365 successive 4-day-long data-arcs to cover the 6 Venusian days or cycles duration of the EnVision mission science phase. The initial state vector at the beginning of each data-arc is taken from the current design of the orbit of the EnVision spacecraft around Venus.

On the basis of this orbit computation, Doppler tracking data are simulated on a daily basis of 3.5 h, and the Doppler noise is modeled as white Gaussian noise with a standard deviation that accounts for the total budget and variabilities due to the SPE angle (Section 2.2.1).

2.2.3. Simulations of the Precise Orbit Determination Process

A comprehensive set of numerical simulations is reported to support the scientific investigation of the EnVision gravity experiment. The numerical simulations were carried out independently with the software *Géodésie par Intégrations Numériques Simultanées* (GINS) developed by the French space agency CNES [10,33] and GEODYN [39]. The simulation of the POD process consists first in building Doppler measurements on the basis of the perturbation of the *initial* force model (hereafter *perturbed* model) and the Doppler noise budget described in Section 2.2.1. The *perturbed* force model takes into account as faithfully as possible the inaccuracies of the force models leading to a realistic simulation of the gravity experiment.

The gravity field is perturbed by applying errors statistically modeled through Normal distributions with a standard deviation of 1-sigma uncertainty of the Magellan/PVO gravity solution [9] for each spherical harmonic coefficient. The real part of the Love number k_2 is set to 0.1, and the imaginary part to zero. Furthermore, each non-gravitational force accounts for errors by scaling randomly the *initial* model through a Normal distribution with a mean value of 1 (e.g., *initial* model) and a realistic standard deviation. The radiation forces are perturbed with a 0.03 standard deviation to consider possible inaccuracies in the spacecraft modeling (e.g., attitude, thermo-optical coefficients of the spacecraft panels) and in the radiation models. The standard deviation for the atmospheric drag is 0.3, which is representative of the average fluctuations of the Venusian thermosphere density observed on the day side (~5%) and night side (~50%) and is also representative of its day-to-day variability at 130–140 km [40]. This standard deviation is a worse case since the atmospheric density is lower at the EnVision orbital altitudes (>220 km).

A further source of dynamical errors is due to Wheel-off-Loading (WoL) maneuvers required to desaturate the reaction wheels used for the attitude control. These maneuvers may lead to uncompensated residual velocities caused by possible thrusters' misalignment. A maximum residual velocity $\mathbf{\Delta V}$ of 1 mm/s (uniformly distributed on the along-track, cross-track and radial directions) is predicted for the current EnVision spacecraft design. These effects are modeled by adjusting the thrust resulting from the impulsive $\mathbf{\Delta V}$ [41] at each daily maneuver, occurring before a tracking period to enable a correct adjustment of this residual $\mathbf{\Delta V}$ effect. This scenario is in line with the requirements of the mission operations.

The discrepancies between the *perturbed* and *initial* (Section 2.2.2) model-based Doppler data are then used to perform a least-squares fit of the force models by adjusting a set of parameters of these models. This fit is performed on each 4-day data-arc through a weighting of the Doppler data based on the assumed noise model (Section 2.2.1). A normal matrix is obtained for each arc, which contains the partial derivatives of the Doppler measurement with respect to local parameters for each arc and global parameters common to all arcs. The local parameters include a scale factor for the drag force and the radiation pressure force, the initial state vector and the three components of the residual thrust generated at each WoL event. The global parameters are the spherical harmonic coefficients of the gravity field to degree and order 180 and the Love number k_2 (real part) and its phase (imaginary part). The global solution is retrieved by combining the normal matrices of all the 365 simulated 4-day-arcs, which cover 6 of Venus' entire cycles, to estimate both local and global parameters.

3. Results

We performed numerical simulations of the EnVision gravity experiment by accounting for a realistic scenario of the gravity experiment. Our results support the enhancements in the estimation of Venus' gravity field that can be achieved with the current radio science and mission configuration.

The drag scale factor is estimated for each arc with an average value of 1 ± 0.017 (1-sigma) over the mission timespan, showing that the initial drag acceleration is precisely retrieved in spite of an a priori perturbation of 30%. The average value of the estimated solar pressure scale factor is 1 ± 0.019 (1-sigma). This is a small improvement with respect to the 3% a priori perturbation, but the adjustment of this force generally displays such a performance [32,33]. The estimated residual thrust at each WoL event corresponds to residual $\boldsymbol{\Delta V}$ solutions, which have accuracies better than 20%.

The estimated spherical harmonic coefficients of the gravity field up to degree and order 180, including the Love number k_2 (real and imaginary part), and their formal uncertainties (or errors) are shown in Table A3 to assess the performance of the future EnVision gravity experiment.

The quality of the estimated gravity field is interpreted in terms of spatial resolution (i.e., degree strength) and uncertainty. The degree strength is the harmonic degree beyond which the error spectra is larger than the power spectra. Both spectra are computed with the root mean square values of all the coefficients and errors at each harmonic degree [42]. To map the spatial resolution, the local degree strength is computed from the spatially projected error of the gravity solution following the method presented in [9].

The minimum degree strength of the EnVision gravity solution is 110 (spatial resolution of 170 km) that is obtained in the southern hemisphere (Figure 1a), and that corresponds to the maximal degree obtained with the Magellan/PVO solution (in the near-equatorial areas [12]). In the northern hemisphere, the expected resolution of the EnVision solution reaches the degree of 160 that enables a spatial resolution of ~120 km (Figure 1a) over regions covered with the lowest altitude of the spacecraft orbit. The spatial resolution map strongly depends, however, on the starting epoch of the science phase and on its initial orbital configuration (see Appendix A and Figure A2).

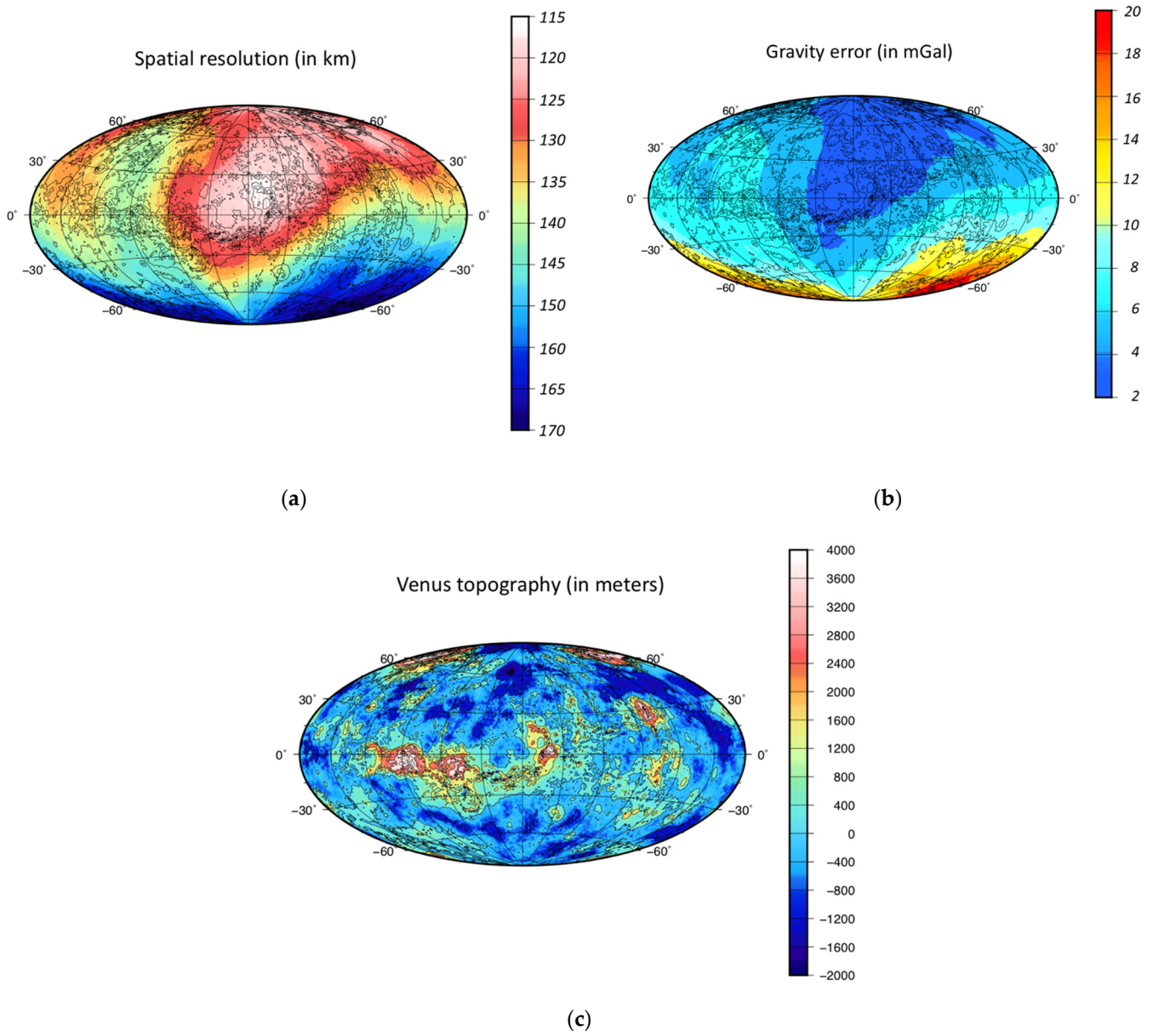


Figure 1. Expected EnVision maps (in Hammer–Aitoff projection) of (**a**) the spatial resolution, (**b**) the cumulated gravity error (1-σ) from the degree 2 to 110. The isocontours of the Venus topography [43] are shown in the background, and (**c**) the Venus topography map (in planetary radius above 6051 km [43]).

To further analyze the expected accuracy of the gravity solution, Figure 1b shows the gravity uncertainty map computed by considering the gravity field to degree and order 110. The uncertainties are <20 mGal everywhere and <10 mGal for 88% of the planetary surface (Table A3), respectively. This is a significant improvement over the Magellan/PVO solution, which shows similar errors but at a lower degree of 70 [8].

The expected 1-σ error of the EnVision Love number k_2 solution is 0.001 (~0.3%) for the real part (Table A3), which is well within the required 3% error to improve our knowledge of the deep interior structure of the planet (Dumoulin et al., 2017). The 1-σ error is representative of the error on the Love number solution since the Doppler post-fit residuals (after fitting the local and global parameters) show values very close to the Doppler noise applied to the simulated Doppler data, meaning that the least-squares fit has extracted most of the information contained in the noisy simulated Doppler data. The 1-σ error of the k_2 imaginary part is 0.001, corresponding to 0.1° for the tidal phase lag

error (Table A3). This error can, however, be larger because of the gravity signal due to the atmosphere (a similar issue arose in the case of Mars [34]).

We also analyzed the effect of the mission duration (4 and 5 cycles or Venusian days instead of 6) on the performance of the gravity field resolution and accuracy as well as of the Love number k_2 and tidal phase lag solutions. The expected EnVision gravity solution is mainly affected if only 4 cycles of tracking data are available in the global inversion (Table A3). This degradation of the gravity field for this shorter mission duration is due to a less uniform surface coverage of the spacecraft ground tracks during tracking and an increased percentage of the noisier tracking data collected during solar conjunctions. A significant impact of the mission duration is also detected for the estimate of the Love number k_2 and tidal phase lag (Table A3).

4. Discussion

These significant improvements expected in the determination of Venus' gravity field will allow us to fully characterize the gravity anomalies associated with most of the geological features, including large tesserae, volcanic rises and coronae, down to a spatial scale of 200 km. In particular, it will increase the coverage for crustal thickness estimates [12], as well as the coverage of a high-resolved gravity field above the coronae. Such a high resolution over the entire planetary surface would allow resolving gravity anomalies above more than half of the coronae. The latest gravity field solution based on the combined analysis of Magellan/POV data provides only information regarding 25% of the coronae [21]. This enhanced coverage of the coronae gravity signatures is required to fully understand the potential role of these structures to initiate subduction of the Venusian lithosphere [19].

Moreover, a uniformly high-resolved gravity map will enable the analysis of the lateral variations of the elastic lithosphere thickness related to local heat flux variations [12,44]. Was the lithosphere thinner in the past, at the time of Tesserae formation and thicker at the time of more recent volcanic rises formation, or could similar geological features form above the lithosphere with various thicknesses? By addressing this outstanding question, we will be able to constrain the heat loss mechanism: episodic vs. equilibrium mode or a different mode [3].

The most powerful tool to characterize the radial structure of a planet (besides seismology) is its moment of inertia, the calculation of which requires the measurement of the precession rate. The moment of inertia of Venus has been computed using estimations of the precession rate derived from Earth-based observations of radar speckles, with an uncertainty of the order of 10% [45]. However, this is not accurate enough to distinguish between the different composition models proposed in the literature for Venus that arise from different accretion scenarios (the two end-member scenarios in terms of FeO mantle content; therefore, the models proposed by [46,47] are in terms of core size). These models, combined with two different temperature profiles in the mantle (Earth-like or hotter) and assuming a core composition similar to Earth's, yield core radius from 2941 to 3425 km with corresponding moments of inertia from 0.342 to 0.327 [14]. In our simulations, we have introduced the estimation of the precession rate from the Envision tracking data. We found a 1-σ error of 70 arcsec.cy^{-1}, leading to a significant improvement of the error on the polar moment of inertia (1-σ = 0.005, which is 1.4% of the central value of the expected range) that allows a tighter constraint on the core size.

As shown in Figure 2, an accuracy of less than 2% (i.e., of the order of $\pm$0.006) for the Love number k_2 helps to determine bounds on the core size. Assuming a fully liquid core, a small Love number k_2 (0.25–0.27) would be the signature of a core size in the lower bound (<3000 km) and of an average viscosity of the mantle larger than 10^{20} Pa s. On the contrary, a large Love number k_2 (0.33–0.35) would be the signature of a large core (>3300 km) and of low average viscosity of the mantle (<10^{20} Pa s). Considering a mantle composition similar to the Earth and intermediate value for mantle viscosity (10^{21} Pa s), a low value of Love number k_2 (<0.27, see [14]) would indicate that the core is entirely solid,

with a viscosity in the lower bound of Earth's inner core estimates (<10^{17} Pa s). In any case, thermal evolution modeling of mantle and core is needed in order to rule out some combinations of the state and size of the core and of the thermal state and composition of the mantle. The determination of the tidal phase lag or Q tidal dissipation factor further constrains these parameters. The error σ_Q on Q is indeed lower than the range $\mathbf{\Delta}Q$ for different averaged mantle viscosity values expected from Venus interior models (Table 1 and Figure A3). This expected error on Q will further constrain the averaged viscosity within one order of magnitude (see Figure 4 in [14]) and along with the k_2 Love number, and the moment of inertia will allow us to place even more constraints on the thermal state and composition of the interior of the planet (Figure 2).

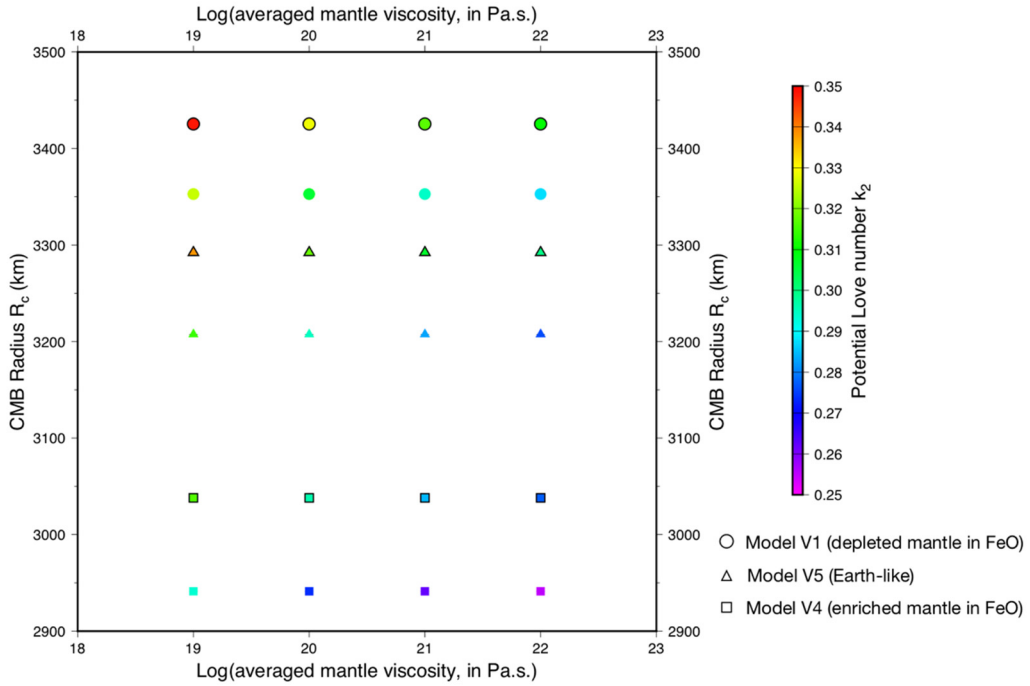


Figure 2. k_2 Love numbers computed for viscoelastic tidal deformation of Venus as a function of the core size and the averaged mantle viscosity. Three different composition models are tested, and two different temperature profiles (an Earth-like profile, symbols with contours, and one hotter without contours). See [14] for a complete description of the computation method, composition models and temperature profiles.

Table 1. Expected error (1-σ) σ_Q of the EnVision solution and theoretical range $\mathbf{\Delta}Q$ of the Venus tidal dissipation factor Q as a function of the average mantle viscosity (see Table A2). The $\mathbf{\Delta}Q$ value for each averaged viscosity represents the variation of the viscoelastic deformation of the Andrade's model used to account for the mantle rheology (see [14]). The σ_Q error is derived from the error on the tidal phase angle $\delta\epsilon$ (0.1° or 0.0017 radian, see Table A3) as follows: $\sigma_Q \approx \mathbf{2}Q^2\delta\epsilon$.

Average Viscosity (Pa.s)	σ_Q**(EnVision)** (1-σ)	$Q \pm \Delta Q$ **(Model)**
10^{22}	24.5	85 ± 35
10^{21}	8.5	50 ± 13.75
10^{20}	2.5	27.5 ± 5
10^{19}	0.9	16.25 ± 3.75

5. Conclusions

The EnVision Radio-Science Experiment aims at providing global mapping of Venus' gravity field, including an accurate estimation of the gravitational tides. The experiment is based on the processing of radio-tracking data acquired by Earth's ground stations during tracking passes dedicated to telemetry and the download of the mission payload data. The

numerical simulations of the EnVision mission scenario demonstrate the scientific achievements that can be accomplished by the Radio Science Experiment with the configuration under study. The resulting gravity field will provide significant accuracy and resolution refinements compared to the Magellan/PVO Venus gravity field. A better Doppler tracking noise (X/X-Ka link against X/X link on Magellan), and especially the six cycles mission duration (against the three cycles dedicated to the gravity field with Magellan), enables dramatic improvements in the knowledge of the short-wavelength gravitational anomalies. A spatial resolution of 170 km is expected globally with local resolutions of 120 km over extensive regions at mid-latitudes. This improvement will provide highly resolved gravity anomalies above most of the geological features (volcanic rises, large tesserae and coronae). The improvement of the solutions of the Love number k_2 (0.3% of error), the tidal phase lag (0.1° of error) and the moment of inertia (1.4% of error) will allow us to better constrain the state and size of the core, as well as the viscosity, thermal state and composition of the mantle. This improvement of the Venus interior structure will then help to better constrain the thermal evolution of the planet, providing a valuable contribution to the EnVision mission.

Author Contributions: Conceptualization, methodology, software, validation, formal analysis, investigation, writing—original draft preparation, writing—review and editing, P.R.; Conceptualization, validation, investigation, writing—review and editing; J.-C.M. Methodology, software, validation, resources, writing—review and editing, C.D.; Software, validation, formal analysis, investigation, writing—review and editing, A.G. All authors have read and agreed to the published version of the manuscript.

Funding: This research was supported by CNES during Phase A of the EnVision mission. A.G. was financially supported by the Italian Ministry of Education, University and Research (MIUR).

Institutional Review Board Statement: Not applicable.

Informed Consent Statement: Not applicable.

Data Availability Statement: Not applicable.

Acknowledgments: The Authors thank the ESA's EnVision study team for numerous fruitful exchanges for implementing the gravity experiment in the Envision mission design, as well as D. Rovelli (ESA) for his valuable help to compute the Envision Doppler noise budget.

Conflicts of Interest: The authors declare no conflict of interest. The funders had no role in the design of the study; in the collection, analyses, or interpretation of data; in the writing of the manuscript, or in the decision to publish the results.

Appendix A

Appendix A.1. EnVision Doppler Noise Budget

Table A1. EnVision Doppler noise budget breakdown (two-way X/X-Ka Doppler measurements at 10 s count time).

Noise Contribution	Ground Station Frequency Stability [a]	Spacecraft Transponder	Earth's Troposphere	Interplanetary Plasma	Ground Station Mechanical Noise	Total Root Square Sum (RSS)
Standard deviation (in mm/s)	0.003	0.024	0.022	0.027 [b] (0.104) [c]	0.009 [d]	0.043 [b] (0.109) [c]

[a] Noise due to the frequency modulation/demodulation system at the receiving station. [b] at inferior conjunction. [c] at Sun-Probe-Earth (SPE) angle of 20°. [d] ESOC, pers. comm., July 2019.

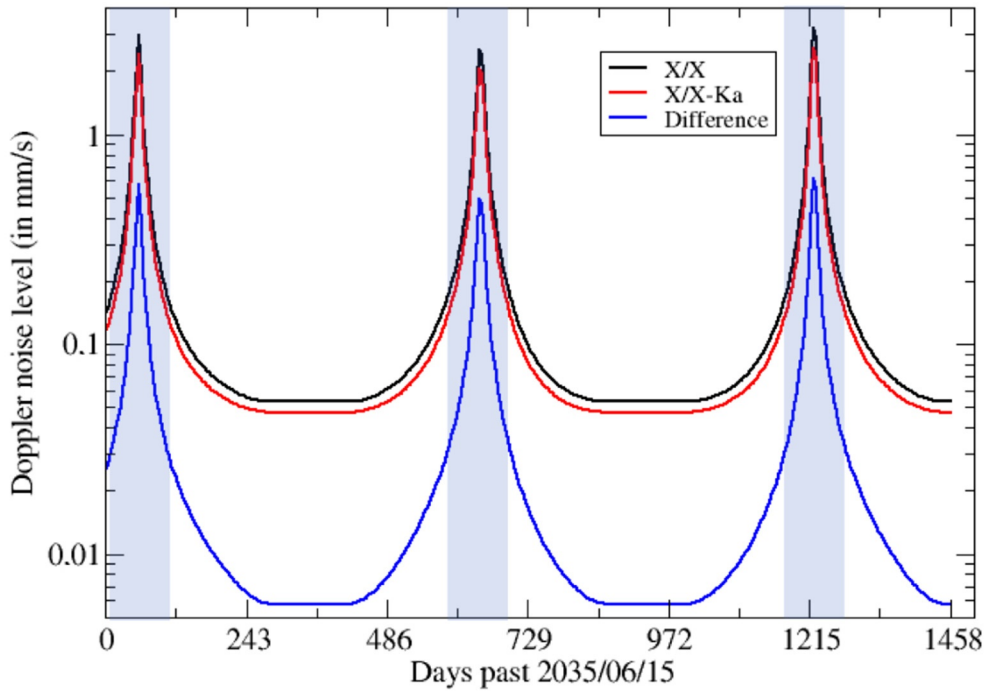
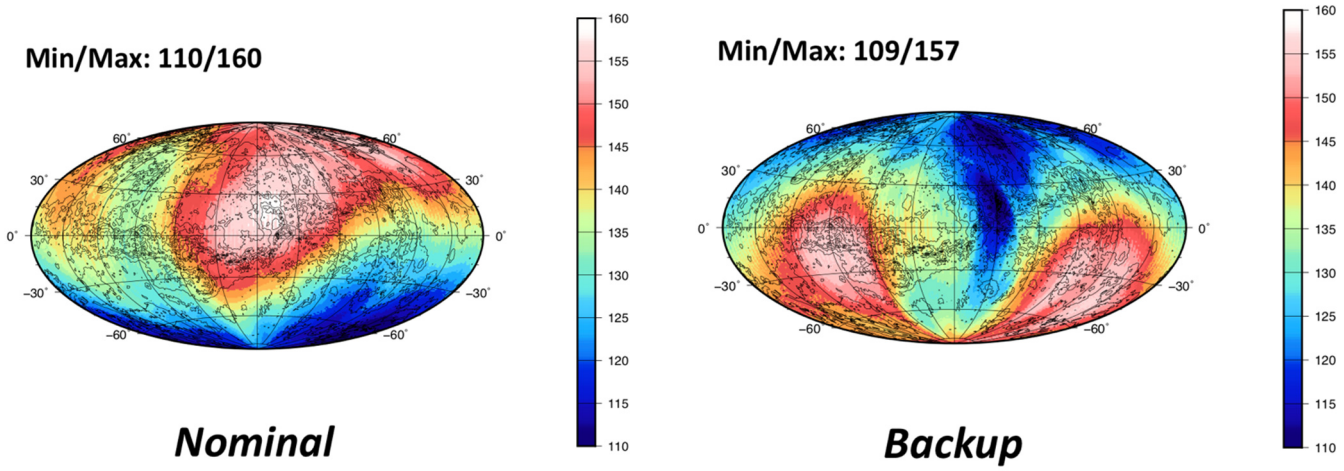


Figure A1. EnVision end-to-end two-way Doppler noise budget (10 s Doppler count time) over Venus' six cycles of the mission science phase (1458 Earth's days) for an X/X-Ka vs. X/X radio-link. The difference between the two link noise levels provides the gain of the Ka downlink frequency on the Doppler noise budget. The light blue areas show the three solar superior conjunction periods occurring during the science phase duration.

Appendix A.2. Influence of Starting Epoch of Science Phase and Initial Orbital Configuration

The starting epoch will constrain the number of POD arcs affected by superior solar conjunctions. The current mission scheduling leads to three solar conjunctions occurring during the science phase (Figure A1). If the starting date is shifted, then only two solar conjunctions would occur. The other constraint regards the initial orbital parameters and, in particular, the pericenter longitude that leads to different orbit evolution. A change in these orbital parameters results in a different local mapping with similar minimum and maximum resolutions. The aerobraking phase needed to reach the science phase orbit after the orbit insertion of the EnVision spacecraft around Venus constrains both the starting epoch and the initial orbit configuration. The mission planning is still investigating backup alternatives that fulfil science and engineering requirements. An example of the predicted gravity field resolution obtained with a backup scenario is given in Figure A2. In this backup scenario, the starting epoch of the science phase is shifted forward by about four months, and only two superior solar conjunctions occur during the 6 Venusian cycles duration of the science phase. The initial orbital configuration also differs from the nominal scenario, and the pattern of the degree strength map changes, although its range is similar (see Figure A2).



(**a**) (**b**)

Figure A2. Expected EnVision maps of the gravity field degree strength (in Hammer-Aitoff projection) for (**a**) the nominal scenario and (**b**) a backup scenario presently under study in phase A of the EnVision mission. The associated spatial resolution map of the nominal scenario is shown in Figure 1. The isocontours of the Venus topography [43] are shown in the background.

Appendix A.3. Venus' Gravity Field and Interior Structure: Model and Simulation Results

Table A2. k_2 imaginary part values and their associated tidal dissipation factor Q and tidal phase lag angle ε values. Each Q value corresponds to the median value computed for four of Venus' average mantle viscosity values (see Figure 4 in [14]). The tidal phase lag angle is derived as $\boldsymbol{\varepsilon \sim 1/2Q}$ and the k_2 imaginary part as $\boldsymbol{k_{2i} = \frac{k_{2r}}{\sqrt{Q^2-1}}}$, with k_{2r} being the k_2 real part (taken here as 0.295 [13]).

Average Viscosity (Pas.s)	Q	ε (Degree)	k_{2i}
10^{22}	85	0.33	0.0034
10^{21}	50	0.58	0.0059
10^{20}	27.5	1.04	0.0107
10^{19}	16.25	1.76	0.0182

Table A3. Planetary surface percentage with a given spatial resolution of the expected EnVision gravity field solution and the error (1-σ) on the expected Love number k_2 and tidal phase lag solutions versus the mission duration.

	Mission Duration		
Resolution (Accuracy)	**4 Cycles**	**5 Cycles**	**6 Cycles**
<170 km	98%	98.5%	100%
<140 km	4%	32%	46%
<20 mGal	97.5%	98.5%	100%
<10 mGal	62%	83%	88%
k_2 Love number Tidal phase lag	0.0014 (0.5%) 0.17° (0.0029 rad)	0.0012 (0.4%) 0.13° (0.0022 rad)	0.001 (0.3%) 0.1° (0.0017 rad)

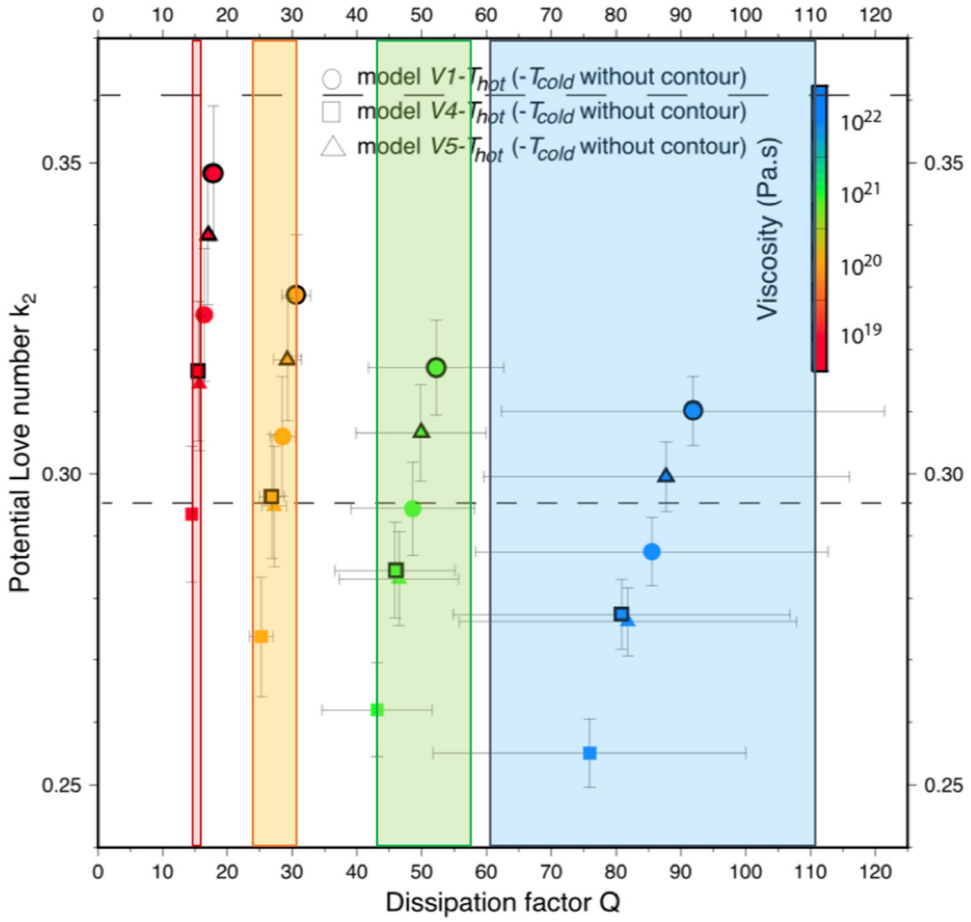


Figure A3. k_2 Love numbers computed for viscoelastic tidal deformation of Venus as a function of the tidal dissipation factor Q (adapted from Figure 4 in Dumoulin et al., 2017). The expected EnVision error of 0.1° on the tidal phase lag (Table A3) corresponds to a Q error σ_Q that is represented as light-colored areas for each Q value representative of a given averaged mantle viscosity (see Table A2). The σ_Q error is derived from the error on the tidal phase lag angle $\delta\epsilon$ as follows: $\sigma_Q \approx 2Q^2\delta\epsilon$.

References

1. Ghail, R.; Wilson, C.F.; Widemann, T.; Titov, D.; Bruzzone, L.; Helbert, J.; Vandaele, A.-C.; Marcq, E.; Dumoulin, C.; Rosen-Blatt, P.; et al. EnVision M5 Venus orbiter proposal. In Proceedings of the European Planetary Science Conference-Division Planetary Science Joint Meeting, Geneva, Switzerland, 15–20 September 2019. Abstract#1611-2.
2. Mocquet, A.; Rosenblatt, P.; Dehant, V.; Verhoeven, O. The deep interior of Venus, Mars and the Earth: A brief review and the need for planetary surface-based measurements. *Planet. Space Sci.* **2011**, *59*, 1048–1061. [CrossRef]
3. Smrekar, S.E.; Davaille, A.; Sotin, C. Venus interior structure and dynamics. *Space Sci. Rev.* **2018**, *214*, 34. [CrossRef]
4. King, S.D. Venus resurfacing constrained by geoid and topography. *J. Geophys. Res. Planets* **2018**, *123*, 1041–1060. [CrossRef]
5. Rolf, T.; Steinberger, B.; Sruthi, U.; Werner, S. Inferences on the mantle viscosity structure and the post-overturn evolutionary state of Venus. *Icarus* **2018**, *313*, 107–123. [CrossRef]
6. Kaula, W.M. Regional gravity fields on Venus from tracking of Magellan cycles 5 and 6. *J. Geophys. Res. Space Phys.* **1996**, *101*, 4683–4690. [CrossRef]
7. Barriot, J.-P.; Valès, N.; Balmino, G.; Rosenblatt, P. A 180th degree and order model of the Venus gravity field from Magellan line of sight residual Doppler data. *Geophys. Res. Lett.* **1998**, *25*, 3743–3746. [CrossRef]
8. Konopliv, A.S.; Sjogren, W.L. *Venus Gravity Handbook*; JPL Publication 96-2 1996; Jet Propulsion Laboratory: Pasadena, CA, USA, 1996.
9. Konopliv, A.S.; Banerdt, W.B.; Sjogren, W.L. Venus gravity: 180th degree and order model. *Icarus* **1999**, *139*, 3–18. [CrossRef]
10. Rosenblatt, P.; Bruinsma, S.L.; Müller-Wodarg, I.C.F.; Häusler, B.; Svedhem, H.; Marty, J.C. First ever in situ observations of Venus' polar upper atmosphere density using the tracking data of the Venus Express Atmospheric Drag Experiment (VExADE). *Icarus* **2012**, *217*, 831–838. [CrossRef]

11. Goossens, S.; Lemoine, F.G.; Rosenblatt, P.; Lebonnois, S.; Mazarico, E. Analysis of Magellan and Venus express tracking data for Venus gravity field. In Proceedings of the 48th Lunar and Planetary Science Conference: The Woodlands, TX, USA, 20–24 March 2017. Abstract#1984.
12. Anderson, F.S.; Smrekar, S.E. Global mapping of crustal and lithospheric thickness on Venus. *J. Geophys. Res. Space Phys.* **2006**, *111*, E08006. [CrossRef]
13. Konopliv, A.S.; Yoder, C.F. Venusiank2tidal Love number from Magellan and PVO tracking data. *Geophys. Res. Lett.* **1996**, *23*, 1857–1860. [CrossRef]
14. Dumoulin, C.; Tobie, G.; Verhoeven, O.; Rosenblatt, P.; Rambaux, N. Tidal constraints on the interior of Venus. *J. Geophys. Res. Planets* **2017**, *122*, 1338–1352. [CrossRef]
15. James, P.B.; Zuber, M.T.; Phillips, R.J. Crustal thickness and support of topography on Venus. *J. Geophys. Res. Planets* **2013**, *118*, 859–875. [CrossRef]
16. Jiménez-Díaz, A.; Ruiz, J.; Kirby, J.F.; Romeo, I.; Tejero, R.; Capote, R. Lithospheric structure of Venus from gravity and topography. *Icarus* **2015**, *260*, 215–231. [CrossRef]
17. Grott, M.; Breuer, D. Implications of large elastic thicknesses for the composition and current thermal state of Mars. *Icarus* **2009**, *201*, 540–548. [CrossRef]
18. Grott, M.; Breuer, D. On the spatial variability of the Martian elastic lithosphere thickness: Evidence for mantle plumes? *J. Geophys. Res. Space Phys.* **2010**, *115*, E03005. [CrossRef]
19. Davaille, A.; Smrekar, S.E.; Tomlinson, S. Experimental and observational evidence for plume-induced subduction on Venus. *Nat. Geosci.* **2017**, *10*, 349–355. [CrossRef]
20. Gülcher, A.J.P.; Gerya, T.V.; Montési, L.G.J.; Munch, J. Corona structures driven by plume–lithosphere interactions and evidence for ongoing plume activity on Venus. *Nat. Geosci.* **2020**, *13*, 547–554. [CrossRef]
21. Hoogenboom, T.; Houseman, G.A. Rayleigh-Taylor instability as a mechanism for corona formation on Venus. *Icarus* **2006**, *180*, 292–307. [CrossRef]
22. Hoogenboom, T.; Smrekar, S.E.; Anderson, F.S.; Houseman, G. Admittance survey of type 1 coronae on Venus. *J. Geophys. Res. Space Phys.* **2004**, *109*, E03002. [CrossRef]
23. Balmino, G.; Moynot, B.; Vales, N. Gravity field model of mars in spherical harmonics up to degree and order eighteen. *J. Geophys. Res. Space Phys.* **1982**, *87*, 9735–9746. [CrossRef]
24. Zuber, M.T.; Lemoine, F.G.; Smith, D.E.; Konopliv, A.S.; Smrekar, S.E.; Asmar, S.W. Mars reconnaissance orbiter radio science gravity investigation. *J. Geophys. Res. Space Phys.* **2007**, *112*, 1–12. [CrossRef]
25. Holmes, D.; Thompson, T.; Simpson, R.; Tyler, G.; Dehant, V.; Rosenblatt, P.; Häusler, B.; Pätzold, M.; Goltz, G.; Kahan, D.; et al. The challenges and opportunities for international cooperative radio science; Experience with mars express and venus express missions. In Proceedings of the AIAA/AAS Astrodynamics Specialist Conference 18, Honolulu, HI, USA, 18–21 August 2008.
26. Ho, C.M.; Morabito, D.D.; Woo, R. Solar corona effects on angle of arrival fluctuations for microwave telecommunication links during superior solar conjunction. *Radio Sci.* **2008**, *43*, 1–13. [CrossRef]
27. Deep Space Network Note 202. *Doppler Tracking*; DSN 810-005, 202, Rev. C. 2019; Jet Propulsion Laboratory: Pasadena, CA, USA, 2019.
28. Iess, L.; Di Benedetto, M.; James, N.; Mercolino, M.; Simone, L.; Tortora, P. Astra: Interdisciplinary study on enhancement of the end-to-end accuracy for spacecraft tracking techniques. *Acta Astronaut.* **2014**, *94*, 699–707. [CrossRef]
29. Graziani, A.; Crewell, S.; Elgered, G.; Jarlemark, P.; Löhnert, U.; Martellucci, A.; Mercolino, T.; Rose, J.; Schween, J.; Tortora, P. Media calibration system for deep space missions: Preliminary design and technical aspects. In Proceedings of the 6th ESA In-ternational Workshop on Tracking, Telemetry and Command Systems for Space Applications, Darmstadt, Germany, 10–13 September 2013.
30. Asmar, S.W.; Armstrong, J.W.; Iess, L.; Tortora, P. Spacecraft doppler tracking: Noise budget and accuracy achievable in precision radio science observations. *Radio Sci.* **2005**, *40*, 1–9. [CrossRef]
31. Notaro, V.; Iess, L.; Armstrong, J.W.; Asmar, S.W. Reducing doppler noise with multi-station tracking: The cassini test case. *Acta Astronaut.* **2020**, *173*, 45–52. [CrossRef]
32. Rosenblatt, P.; Lainey, V.; Le Maistre, S.; Marty, J.C.; Dehant, V.; Pätzold, M.; Van Hoolst, T.; Häusler, B. Accurate Mars express orbits to improve the determination of the mass and ephemeris of the Martian moons. *Planet. Space Sci.* **2008**, *56*, 1043–1053. [CrossRef]
33. Marty, J.C.; Balmino, G.; Duron, J.; Rosenblatt, P.; Le Maistre, S.; Rivoldini, A.; Dehant, V.; Van Hoolst, T. Martian gravity field model and its time variations from MGS and Odyssey data. *Planet. Space Sci.* **2009**, *57*, 350–363. [CrossRef]
34. Konopliv, A.S.; Yoder, C.F.; Standish, E.M.; Yuan, D.-N.; Sjogren, W.L. A global solution for the Mars static and sea-sonal gravity, Mars orientation, Phobos and Deimos masses, and Mars ephemeris. *Icarus* **2006**, *182*, 23–50. [CrossRef]
35. Genova, A.; Goossens, S.; Lemoine, F.G.; Mazarico, E.; Neumann, G.A.; Smith, D.E.; Zuber, M.T. Seasonal and static gravity field of Mars from MGS, Mars Odyssey and MRO radio science. *Icarus* **2016**, *272*, 228–245. [CrossRef]
36. McCarthy, D.D.; Petit, G. (Eds.) *IERS Conventions (2003)*; IERS Technical Note 32; BKG: Frankfurt/Main, Germany, 2004.
37. Folkner, W.F.; Boggs, D.H.; Williams, J.G. *Planetary Ephemeris DE430*; IOM 343-R; Jet Propulsion Laboratory: Pasadena, CA, USA, 2013.

38. Hedin, A.E.; Niemann, H.B.; Kasprzak, W.T.; Seiff, A. Global empirical model of the Venus thermosphere. *J. Geophys. Res. Space Phys.* **1983**, *88*, 73–84. [CrossRef]
39. Pavlis, D.E.; Wimert, J.; McCarthy, J.J. *GEODYN II System Description (Vols. 1–5)*; SGT Inc.: Greenbelt, MD, USA, 2013.
40. Müller-Wodarg, I.C.F.; Bruinsma, S.; Marty, S.B.J.-C.; Svedhem, H. In Situ observations of waves in Venus's polar lower thermosphere with Venus express aerobraking. *Nat. Phys.* **2016**, *12*, 767–771. [CrossRef]
41. Rosenblatt, P.; Marty, J.C.; Perosanz, F.; Barriot, J.P.; Van Hoolst, T.; Dehant, V. Numerical simulations of a Mars geodesy network experiment: Effect of orbiter angular momentum desaturation on Mars' rotation estimation. *Planet. Space Sci.* **2004**, *52*, 965–975. [CrossRef]
42. Kaula, W.M. *Theory of Satellite Geodesy*; Blaisdell: Waltham, MA, USA, 1966.
43. Rappaport, N.J.; Konopliv, A.S.; Kucinskas, A.B.; Ford, P.G. An improved 360 degree and order model of Venus topography. *Icarus* **1999**, *139*, 19–31. [CrossRef]
44. Smrekar, S.E. Evidence for active hotspots on Venus from analysis of Magellan gravity data. *Icarus* **1994**, *112*, 2–26. [CrossRef]
45. Margot, J.-L. Earth-based radar observations of the spin axis orientation, spin precession rate, and moment of inertia of Venus. In Proceedings of the European Planetary Science Conference-Division Planetary Science joint meeting, Geneva, Switzerland, 15–20 September 2019. Abstract#412-3.
46. Lewis, J.S. Metal/silicate fractionation in the solar system. *Earth Planet. Sci. Lett.* **1972**, *15*, 286–290. [CrossRef]
47. Ringwood, A.E. *Composition and Origin of the Earth. Canberra, Research School of Earth Sciences 1977*; Publication No 1227; Australian National University: Canberra, Australia, 1977.